International Journal of Applied Earth Observation and Geoinformation 134 (2024) 104154

Contents lists available at ScienceDirect

International Journal of Applied Earth Observation and Geoinformation

journal homepage: www.elsevier.com/locate/jag

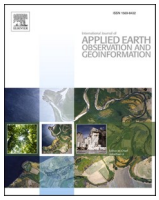

Framework for UAV-based river flow velocity determination employing optical recognition

Andrius Kriščiūnas [a], Dalia Čalnerytė [a], Vytautas Akstinas [b], Diana Meilutytė-Lukauskienė [b], Karolina Gurjazkaitė [b], Rimantas Barauskas [a]

[a] Department of Applied Informatics, Kaunas University of Technology, Lithuania
[b] Laboratory of Hydrology, Lithuanian Energy Institute, Lithuania

ARTICLE INFO

Keywords:
Unmanned aerial vehicle
Aerial video
River flow velocity
Optical flow
Indirect measurements

ABSTRACT

The determination of river velocity is important for hydromorphological analyses and river monitoring systems. Indirect measurements of river velocity using videos recorded by unmanned aerial vehicles (UAV) allow fast and cost-effective processing of information about the river stretch. This paper presents a method for computing flow velocity of the river surface using deep supervised model RAFT to determine the optical flow in combination with image pre-processing by convolutional operations. Moreover, the windiness coefficients and variance score were proposed to evaluate reliability of the collected data and the obtained results of optical flow detection. Various image pre-processing techniques were applied, namely the selection of the analysed area and the number of convolutional operations to select the one with the lowest variance score. This score represents the consistency of the river flow velocity during the video and can be used to filter out unreliable results. The numerical experiments were performed using the videos and directly measured velocity values of 4 shallow rivers in Lithuania collected during the field surveys. The optical velocity estimation method showed good correspondence to the directly measured values for the velocity range from 0 m/s to 0.8 m/s in the points with low variance score up to 0.192 that represents the first quartile of the variance. The optical flow method tends to underestimate the velocity up to 0.5 m/s for the quartiles with the higher variance scores. It was shown that in most cases the lowest variance score value was obtained using pre-processing techniques without convolutional operations. However, the need to analyse various pre-processing techniques arises from the different origin of the objects moving on the river surface.

1. Introduction

Rivers, with their complex water movements influenced by elevation gradients, morphology and wind dynamics, require accurate and precise determination of flow velocity for riparian ecosystem monitoring (Rusnák et al., 2022), water resource planning and disaster management during floods and droughts. Traditional methods such as current meters and floats have their limitations. These include high labour requirements, limited spatial coverage, challenges in extreme conditions, temporal limitations, high costs, reliance on human interpretation and difficulties in measuring subsurface velocities (Di Baldassarre and Montanari, 2009; Le Coz et al., 2012; Figuérez et al., 2021). To overcome these hurdles, unmanned aerial vehicles (UAV) (Kinzel and Legleiter, 2019; Eltner et al., 2020), satellites (Bjerklie et al., 2018; Zhang et al., 2022) and radar observations (Fulton et al., 2020) offer a transformative solution that improves the estimation of various river characteristics. The indirect estimation of river flow velocity enables the collection, processing and analysis of data over the entire river stretch in real time and reduces time and human-power recourses. Satellite-based approaches, which are often used in large-scale hydrological studies, are proving particularly valuable for the assessment of large water bodies. Meanwhile, unmanned aerial vehicles (UAVs) have gained importance in hydrology due to their high spatial and temporal resolution, which, unlike satellites, enables data collection for smaller water bodies as required (Vélez-Nicolás et al., 2021). UAVs can be used to estimate velocity fields over natural rivers (De Schoutheete et al., 2019; Koutalakis et al., 2019). These studies emphasise the efficiency of ground control points in rectifying and stabilising images for accurate analysis. Furthermore, the method developed to measure the surface velocity of rivers using a moving drone showed wide applicability for broad water bodies where the installation of a reference point is impractical (Yu and Lee, 2022).

E-mail address: vytautas.akstinas@lei.lt (V. Akstinas).

https://doi.org/10.1016/j.jag.2024.104154
Received 26 May 2024; Received in revised form 9 August 2024; Accepted 5 September 2024

Many applications for indirect estimation of flow velocity in rivers are based on particle tracking (Koutalakis and Zaimes, 2022) or optical flow algorithms in combination with deep learning algorithms (Ho et al., 2023; Jyoti et al., 2023). The estimation of the flow velocity at the river surface can be done using particle tracking or particle image velocimetry methods from videos recorded with terrestrial or aerial cameras (Eltner et al., 2020) or thermal image time series (Legleiter et al., 2017; Kinzel and Legleiter, 2019). The comparative analysis of different image velocimetry techniques to determine the flow velocity of rivers from UAV data has shown practically acceptable results (Wijaya et al., 2023). The particle tracking and particle image approaches are limited by the fact that natural or artificial tracers must be present on the water surface, in contrast to the optical flow method, which overcomes this issue by estimating the displacements of individual pixels (Jyoti et al., 2023). To estimate the flow velocity at the surface, an optical flow method with automatic feature detection and posteriori filtering was presented to obtain realistic trajectories (Tauro et al., 2018). Optical methods are sensitive to a variety of environmental conditions such as lighting, wind, debris and others (Jyoti et al., 2023) and the pre-processing steps should be implemented before the analysis or considered in the development of the model. The direct cross-correlation technique in particle image velocimetry has been replaced by convolutional neural networks (CNNs) to reduce the effects of environmental noise such as non-uniform illumination (Ho et al., 2023). Similarly, generative adversarial networks (GAN) and CNNs have been used to improve image quality and predict the flow velocity of rivers (Wang et al., 2022). The Deep supervised optical flow velocity model RAFT (Teed and Deng, 2020) was supplemented with an attention mechanism and position encoding to make the velocity estimation more robust to reflections and flicker (Cao et al., 2022). A framework combining hydrodynamic modelling and synthetic particle generation (Legleiter and Kinzel, 2024) were developed to provide an environment for comparing different velocimetry algorithms under different conditions.

This paper presents a method for pre-processing UAV images to improve the flow patterns recognition. The research focuses on estimating the flow velocity at the surface of a shallow river using aerial videos captured by a drone. The main aim of this study is therefore to estimate the flow velocity as a flow vector considering environmental factors at a given point supported by direct measurements. The proposed technique is based on the state-of-the-art recurrent neural network architecture RAFT, where the model is trained and tested on various annotated video stream datasets such as Kitti (Geiger et al., 2013) and Sintel (Mayer et al., 2016). Of course, such a model can be trained with river flow data and fully adopted for the river scale context. The motivation behind determining the flow velocity at a target point is based on the following factors:

- the automatic processing of high-resolution images of short local segments and the combination of the results allows long river stretches to be analysed with reasonable computational resources, which would be impossible if long river stretches were processed directly;
- collecting high-resolution images in a local area does not require expensive specialised equipment that is needed for capturing large geographical areas;
- local conditions may require different image pre-processing techniques, and specific point-based flow velocity estimation in small areas may be more appropriate.

2. Methodology

This section presents the general workflow of a research methodology, including data collection, its calibration and georeferencing, optical flow measurement in the river and analysis of the results. The general scheme of the methodology is shown in Fig. 1. After the steps of data collection, calibration and georeferencing, the river flow velocity was estimated using the optical flow method in the environment of each point of interest for the pre-processed images of different time intervals. The set of the obtained results was employed to evaluate the reliability of the velocity estimation results. The obtained results are generalised for the entire river stretch.

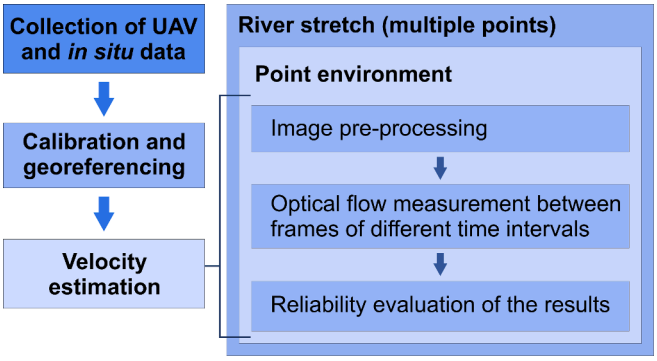

Fig. 1. The general scheme of the proposed methodology.

2.1. Data collection

The river stretches of four Lithuanian rivers were selected for the determination of the flow velocity on the basis of drone imagery (video records). Lithuania falls within the mid-latitude climate zone, which is characterised by a humid continental climate with predominantly warm summers. Accordingly, the average annual temperature for the area is 7.4 °C and the annual precipitation is 695 mm (Lithuanian Hydrometeorological Service under the Ministry of Environment (2021)). Although precipitation is evenly distributed throughout the year, there is slightly more precipitation in the summer months than in the other months. These conditions ensure that the rivers are supplied with water all year round. The selected river stretches represent different hydrological and physico-geographical conditions at the local scale, as the study sites are located in different hydrological regions and consist of different components in the riverbed, from clean riverbeds to dense aquatic vegetation and the presence of boulders. Such a selection includes the diversity of possible natural hydraulic conditions in order to avoid monotonous and uniform flow conditions and to adapt the artificial intelligence (AI) model to different natural flow situations. Examples of the images of the river stretch with reference to their locations can be found in Fig. 2.

All study data was collected during the field surveys. The collected data consisted of hydrological parameters and drone videos over the target area. The Valeport 801 electromagnetic flowmeter was used to measure river flow velocity. Point measurements of surface flow velocity were taken at 10 cm depth for 10 s to estimate the average velocity of surface movement. The geographic coordinates of each point were collected using the GeoMax Zenith 40 GNSS GPS receiver and X-PAD Ultimate Survey software and georeferenced with the flow velocity measurements in ArcGIS 10.5. In addition, the coordinates of 4 ground control points (GCP) were measured for each water surface to integrate the aerial imagery into a known geographic coordinate system and to maintain the scale for estimating flow velocity from optical data. The accuracy of the coordinates is ± 0.015 m. The aerial videos were captured using a DJI Mavic 3 multispectral drone with a 4/3-inch CMOS sensor RGB camera with a resolution of 3840 x 2160 pixels.

In order to evaluate the instantaneous changes in velocities at a given point of the river caused by physical uncertainties such as turbulence or visual changes in the river surface due to wind gusts or cloud cover, two independent video streams (with different viewing positions) longer than 25 s were collected at each stretch. Later, each stream was divided into 3 independent sub-streams of 5 s, using a time interval of 5 s between the sub-streams, see Fig. 3. This finally leads to 6 independent

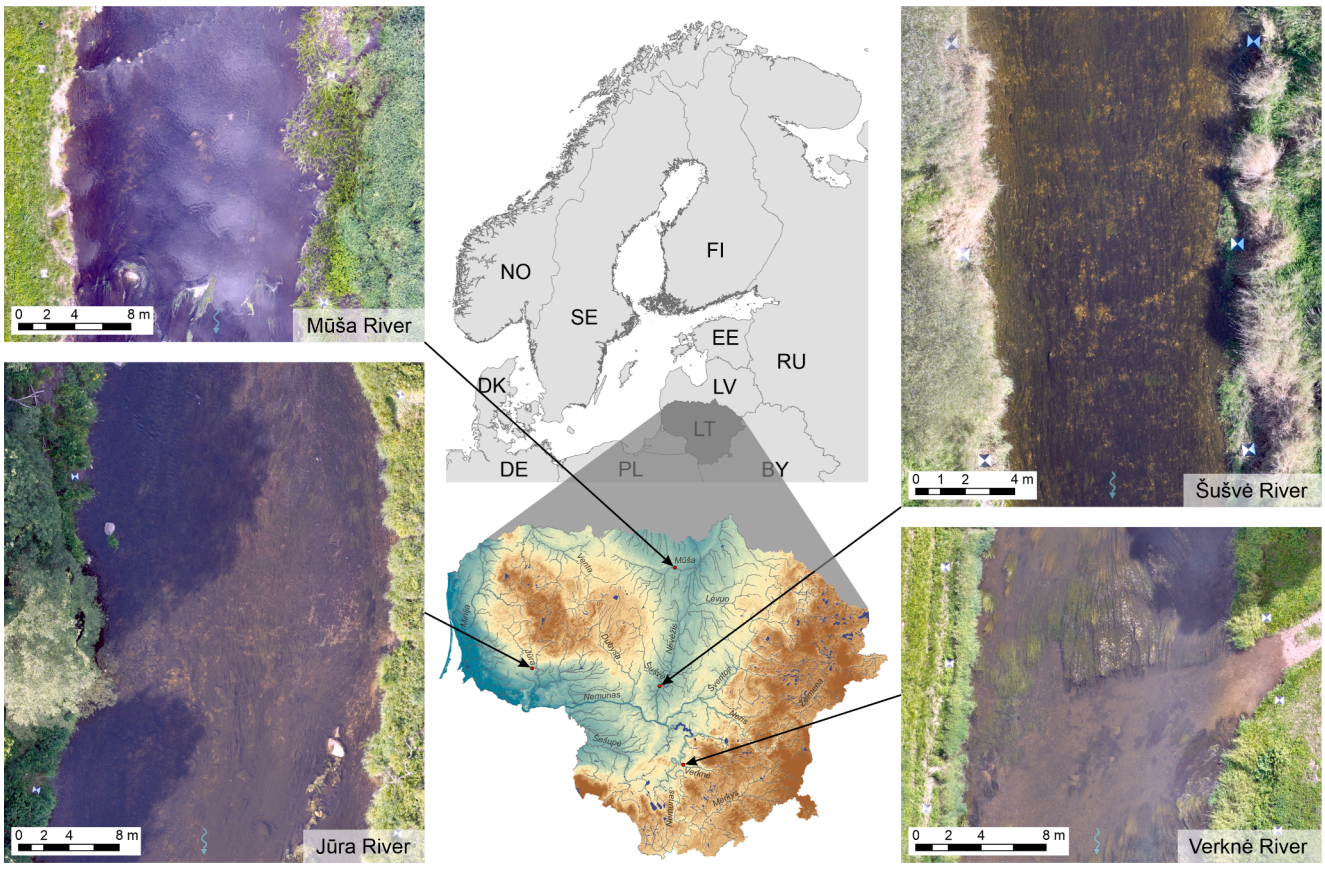

Fig. 2. Study area and objects.

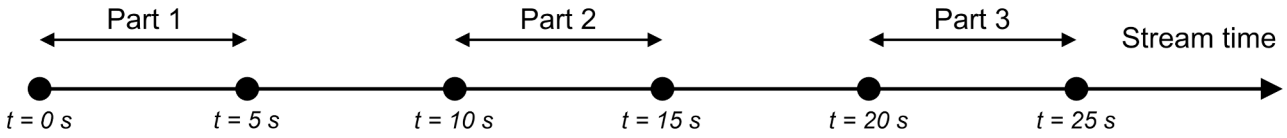

Fig. 3. The scheme of splitting video into the sub-streams.

sub-streams (5 sec equal to 150 frames) for each location to be analysed.

The flow direction of the river was not determined during the field study. Therefore, only the comparison between the measured and optically estimated scalar values was carried out and the calculated flow direction was optically analysed.

2.2. Data calibration and georeferencing

As mentioned in 2.1, the data for each region was collected from a different perspective. An example of the initial orientation of the video view for the location Jūra-S2 can be found in Fig. 4 (in the left part). The streams for each location were orientated approximately perpendicular to the river. The accuracy of the coordinates is ± 0.015 m. To obtain a uniform georeferenced dataset, the first frame for each flow was scaled to 1px = 0.01 m and the centres of the markers were linked to the exact pixels in the frame, see Fig. 5.

It should be noted that despite the stabilisation systems used in UAV, the position of the drone may change slightly over time due to the wind and that the georeferenced information based on the first frame may contain errors. In order to be able to calibrate the entire video stream properly, a 200 x 200 pixel image was cropped for each frame based on the GCP position marker of the first frame. The image size represents to 2 x 2 m and was chosen assuming that the displacement does not exceed 1 m. Using the optical flow detection model (RAFT, see section 2.3), the shift of the marker centre between the frames was automatically calculated and the pixels of the marker centres were adjusted for the next frames before georeferencing. Fig. 5 shows the position changes of the Jūra-S2 marker in an interval of 5 s, whereby the 150th frame is visualised with the determined marker centre (red point). The blue point represents the position of the marker centre in pixels of the first frame, the black points represent the movement of the marker centre in time (changes between the 0 and 150 frames).

To evaluate the level of windiness at different locations, the averaged displacement of the ground control points (GCP) within the frames was measured:

$$u_w = \frac{\sum_{i=1}^{N} \sqrt{|x_i - x_{i-1}|^2 + |y_i - y_{i-1}|^2}}{N-1} \quad (1)$$

here, x and y represent the coordinates of the GCP centre in the i-th frame of N frame series, u_w for the averaged displacement of the GCP point in the image during the video stream. It should be noted that such calculations represent the wind conditions in the exact position and are highly dependent on the initial conditions of the experiments. For example, different characteristics of the UAV stabilisation or differences in the quality of the georeferenced images may cause changes that cannot be attributed to the wind. In this case, however, the wind conditions were not measured during the field surveys, and the metric u_w

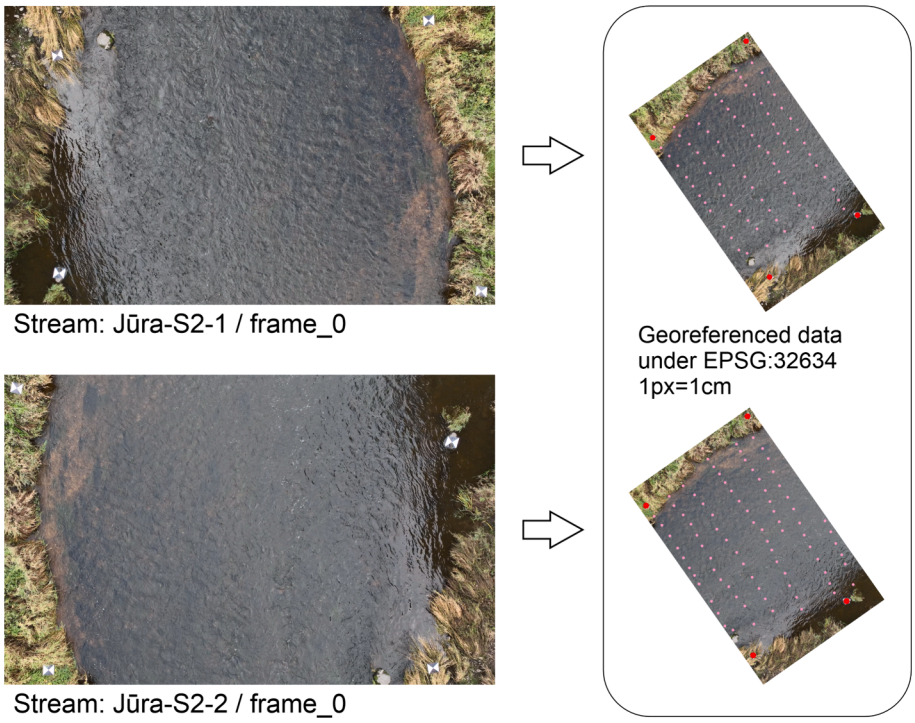

Fig. 4. Example of georeferencing the first frame of Jūra-S2 stream.

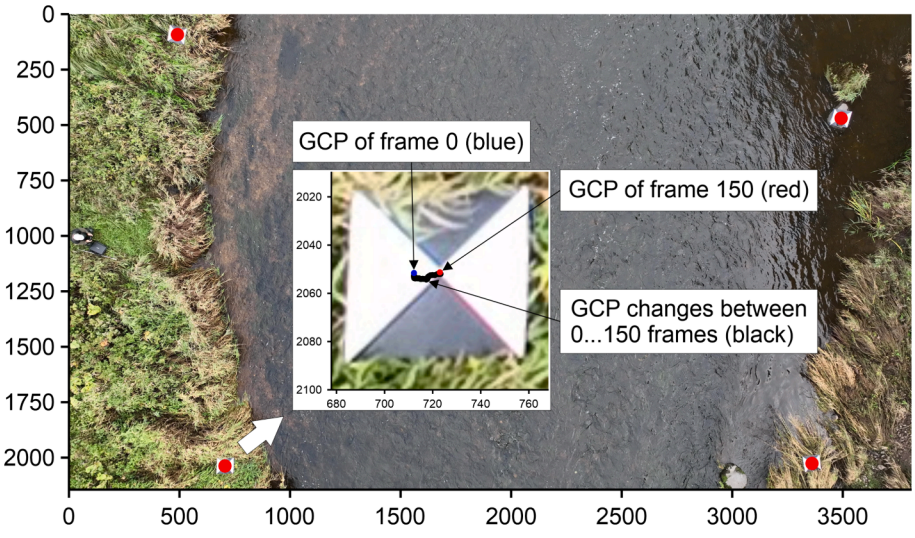

Fig. 5. Example of the georeferencing of the Jūra-S2 stream according to the first and last frame.

was calculated to eliminate wind-independent factors, as the same drone was used at height range of 10.5–31.0 m above the surface to capture the video streams.

2.3. Optical flow velocity

Determining the velocity of a river from an aerial video leads to the problem of optical flow velocity (Horn and Schunck, 1981), since changes in the exact point between frames in pixels directly represent point displacements. In this study, RAFT was selected as the core model for the optical flow detection problem (Teed and Deng, 2020).

Using the pair of two frames labelled as I_1 and I_2, the model provides the optical flow map $\left(f^1, f^2\right)$ in which each pixel with coordinates (x, y) of I_1 is expressed as a pixel (x', y') in I_2 as:

$$(x', y') = (x + f^1(x), y + f^2(y)) \tag{2}$$

If the images are georeferenced with the actual distance in metres d_a between the pixels, and the time interval between the frames are known t_f, the actual velocity of the exact pixel between two frames can be expressed as follows:

$$v_{x,y} = \left(\frac{f^1(x) * d_a}{t_f}, \frac{f^2(y) * d_a}{t_f}\right) \tag{3}$$

here $v_{x,y}$ is the velocity vector at the pixel (x, y). Finally, the scalar velocity at the exact pixel $\widetilde{v}_{x,y}$ is expressed as an Euclidean vector norm $\widetilde{v}_{x,y} = \|v_{x,y}\|$ and is measured in m/s.

2.4. Optical flow velocity measurement at river

In this study, the objective was to create a static map of the flow velocities on the surface of the selected river segment. The main assumption is that the velocity in the same area maintains the same direction and magnitude over a short period of time. An example of the sequence of the area around the point of interest (Mūša-S2) is provided in Fig. 6.

The calculated velocity between frames at time t_0 and frames at time $t_0 + k\Delta t$ for small values of k is, as expected, the same. Here Δt is the time interval between two adjacent frames, k represents the number of frames from the first frame t_0. It is important to maintain a small value of k, as it may be impossible to visually recognise movement in images with larger time interval. However, due to environmental factors, such as wind gusts, the calculated velocities differ between the pairs of frames. Thus, a set of velocities V is created out of the scalar velocity values $\widetilde{v}_{t_0,t_0+i\Delta t}$, $i = \overline{1,k}$ calculated in the area of interest between the frame at time t_0 and k frames ahead:

$$V = \{\widetilde{v}_{t_0,t_0+\Delta t}; \cdots; \widetilde{v}_{t_0,t_0+k\Delta t}\} \tag{4}$$

In this study, the level of the velocity variability is measured as a ratio of the standard deviation σ_V and mean μ_V of the set V and interpreted as the velocity variance score. The smallest value of the variance score means that the velocity values calculated for the same point and different pairs of frames are the most similar. Such a value therefore represents the most accurate and reliable results. The variance score r is expressed as:

$$r = \frac{\sigma_V}{\mu_V} \tag{5}$$

In general, optical flow can be detected as an entire moving surface or as individual particle movements. If the velocity is recognised as a moving surface, the velocity of the exact point or the velocity averaged over a small area may be regarded as the velocity $\widetilde{v}$ at a point. However, if the velocity is determined from the moving particles around the point, the velocity of a single particle determines the velocity of the river (flow). The velocity $\widetilde{v}$ is calculated as the maximum value of the velocities in the analysed area and prevents the risk of not detecting the movement at a certain point by using the optical flow:

$$\widetilde{v} = \underset{v \in P}{argmax}(\|v\|) \tag{6}$$

here P means the set of pixel velocities in the area to be analysed. Of course, a larger area can lead to more generalised results, which is not preferred as the velocity at the exact point is an object of interest. In this case, therefore, the size of the area to be analysed is a parameter that is later selected according to the variance score r. From the square image NxN pixels, the area of interest is obtained by creating a circular mask of radius R proportional to N divided by the coefficient α. Examples of a full-surface velocity map and an area limited by a circular mask with $\alpha = \{2, 3, 4\}$ can be found and are provided in Fig. 7.

If the data set used in the analysis is large enough, the image pre-processing part can be included in the artificial intelligence (AI) model to learn which pattern best fits the situation to determine the flow. However, in our case, the training data is limited and the different pre-processing techniques are used with the already trained RAFT model, while the best one for the exact position is obtained using the variance score. Having a large dataset would enable to adjust the RAFT model for the specific conditions, but the data collection procedure is expensive, and it is not possible to augment the dataset to the size that enables to fully train the model. The aim of the image pre-processing was to enlarge moving small particles in the river flow to improve their detection with the RAFT model. The initial frames I_1 and I_2 were modified according to the masks calculated as their threshold differences $D_1 = I_1 - I_2$ and $D_2 = I_2 - I_1$ and magnified using c 2D convolution operations with a filter of a 3x3 matrix of ones. An example of the results for different c values is presented in Fig. 8.

In general, various pre-processing techniques can be applied. In this research, the pre-processing is based on analysing the optical flow in different areas and performing a different number of convolutional operations to enlarge the moving particles. Therefore, the set of image pre-processing cases is defined as M and contains all possible combinations of:

a) different radiuses of the circle under analysis R;
b) logical variable $diff \in \{0; 1\}$ which represents whether the image pre-processing part with calculating threshold differences and convolution operations is applied;
c) $c \in C$, here C is the set of number of convolutions if $diff$ value is equal to 1.

The applied combination m_a is the one that results in the minimum variance score:

$$m_a = \underset{m \in M}{argmin}(r_m) \tag{7}$$

here, the r_m is a variance score obtained using $m \in M$ image pre-processing method. The method for selecting the image pre-processing technique m_a for the specific point when the velocity between the initial frame at time t_0 and $k = \{2, 4, 6\}$ frame intervals with radius $R = N/2$ is calculated and visualised in Fig. 9. The top left part shows the sequence of the initial frames. A scheme for determining the optical flow between the frames when image pre-processing has not been used, $diff = 0$ is presented in the left bottom part. The right part of Fig. 9 disclosed

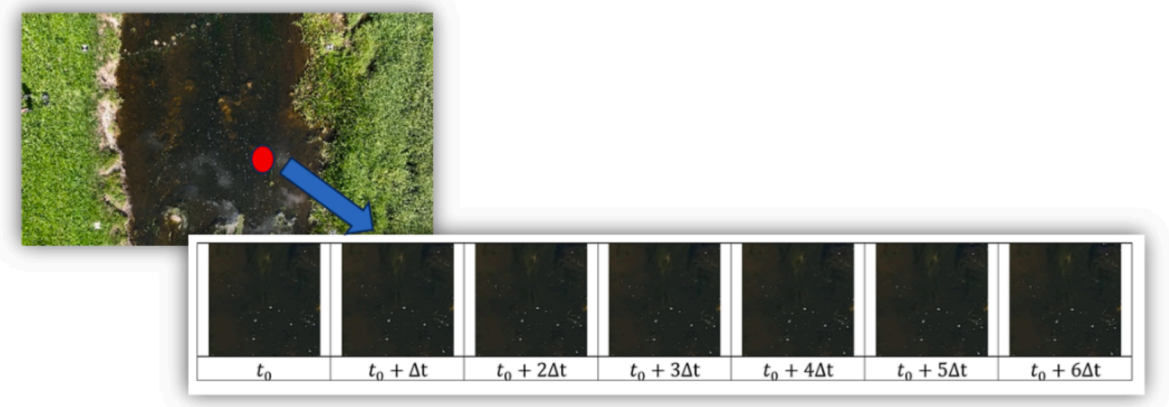

Fig. 6. A sequence of images generated based on the point of interest.

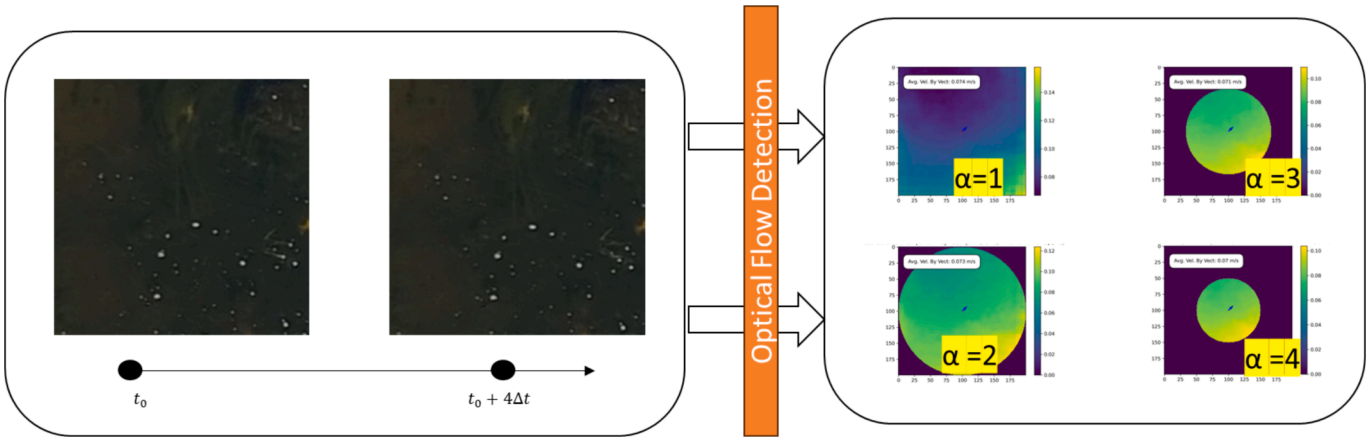

Fig. 7. Scheme of optical flow detection between two frames and resulting velocity maps for areas limited with the velocity maps.

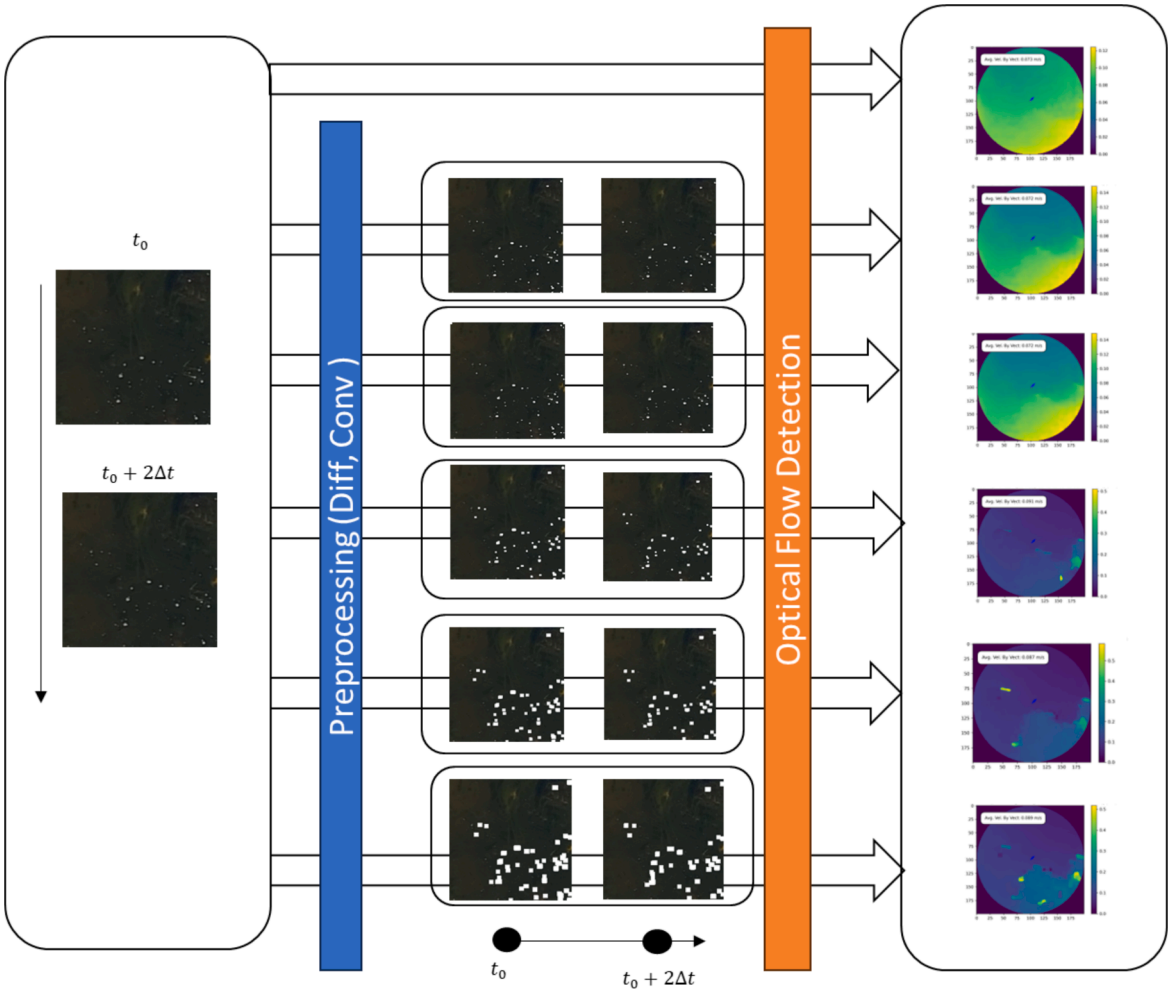

Fig. 8. Schematic of pre-processing of images using convolution operations and the resulting velocity maps for a circular mask R=N/2.

the case with enabled image pre-processing, $diff = 1$, $c = 4$ applied convolution operations. Finally, the lower part of Fig. 9 represents the selection of $\widetilde{v}$ as the averaged value of the calculated velocity with the minimum variance score r.

This procedure can easily be extended to other sequences to be processed. In general, several video streams for geographic point p may be combined to obtain the most suitable f_m for the exact location. Here, the *vel* set used to calculate the reliability score can consist of frames starting at different initial times and even independent video streams, see Section 2.1 and 2.3.

3. Results

3.1. Data collection, pre-processing and evaluation of windiness

The study was conducted for data streams from 4 different rivers,

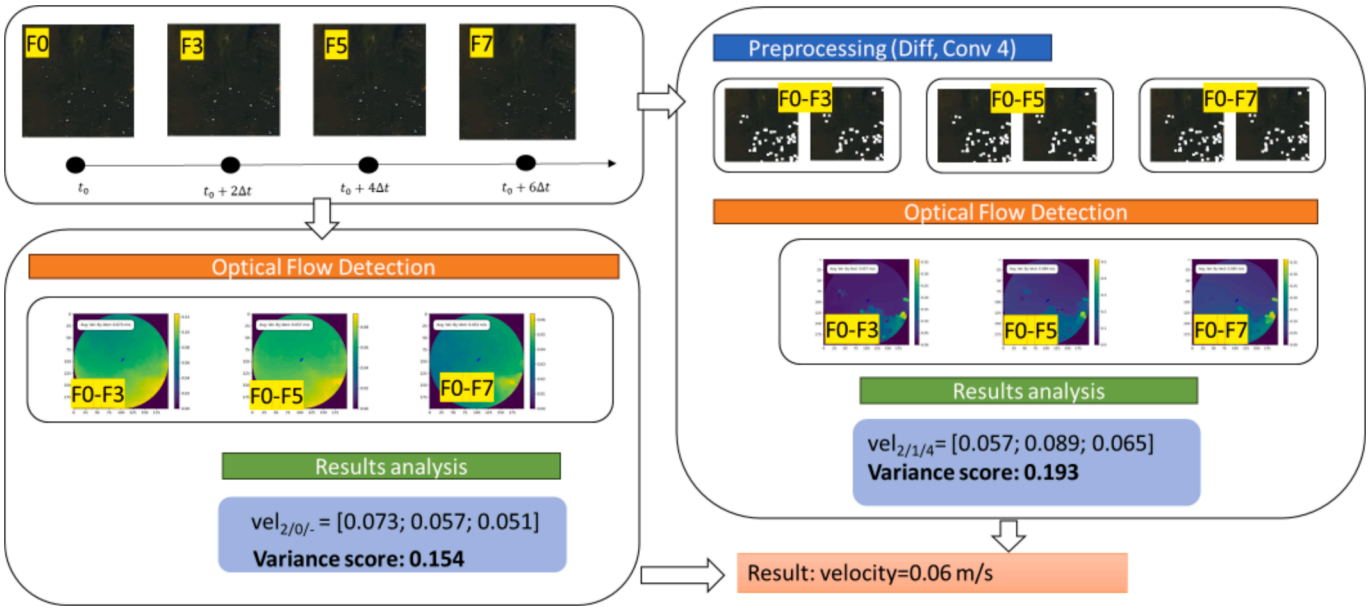

Fig. 9. Selection procedure of the image pre-processing technique. The upper left part shows the initial frames, the bottom left part shows the results of the optical flow recognition, the right part disclosed the results of the optical flow recognition after applying the convolution. The lower indices represent α, diff and *c* values respectively. The result is the averaged value of the calculated velocities with minimum variance score evaluation.

each with 2–4 water surfaces at the same discharge to cover areas with various hydrodynamic features, using the methodology described in sections 2.1 and 2.2 (Table 1). To estimate the movement of the drone during data collection, the formula (1) was applied to calculate the windiness coefficient and evaluate the reliability of the results. The average windiness coefficients were calculated for all GCPs of each river surface (4 GCPs per surface and stream) and for video streams consisting of 6 streams with 5 s each (Table 1). The highest windiness coefficients were determined for the Šušvė River surfaces. The range of estimated coefficients was between 4 and 8, describing rough flight conditions that strongly affected the quality of the collected data and also made frames processing difficult. This described the high instability of air movements and the effects of wind gusts during the field surveys. In contrast, the surfaces of the Mūša River showed the best results in terms of windiness conditions. The windiness coefficients on both studied surfaces did not exceed 0.74 and were characterised by low variability.

To demonstrate the instability caused by the wind, Fig. 10 visualises the movement of the GCP within the frame during the cases with the lowest (Mūša-S2) and highest (Šušvė-S1) windiness coefficients for the first five seconds. The GCP movement for Mūša-S2 showed almost perfect results, as all 150 video frames fitted within the centre of the ground marker with very low relative and absolute distribution. In contrast, the frames for the Šušvė-S1showed a large dispersion with respect to the GCP that moved ± 10 cm. This emphasises the importance of the effects of environmental factors such as wind and its gusts on the reliability of the collected data. This analysis can be a solution for the primary overview of the drone footage to determine and select the most suitable video streams with the smallest windiness coefficient for subsequent processing. It also enables to mitigate the impact of the drone instability by adjusting the necessary frame part with respect to the GCPs. However, the other environmental factors such as lighting, debris, and water turbidity can also result in a high variance score.

Table 1
Windiness coefficients for different data streams.

No.	River-Surface	Discharge (m^3/s)	Windiness coefficient	Flight height (m)
1.	Jūra-S1	3.24	1.97	19.2
2.	Jūra-S2	3.24	2.07	17.2
3.	Jūra-S3	3.24	1.87	19.7
4.	Mūša-S1	0.548	0.74	24.1
5.	Mūša-S2	0.548	0.62	31.0
6.	Šušvė-S1	0.491	8.03	10.6
7.	Šušvė-S2	0.491	7.56	13.0
8.	Šušvė-S3	0.491	6.9	12.5
9.	Šušvė-S4	0.491	4.01	12.8
10.	Verknė-S1	1.42	2.54	21.9
11.	Verknė-S2	1.42	5.21	16.2

3.2. Image pre-processing

Different pre-processing methods were used to minimise the error in the variance score. All points from the dataset were processed with different pre-processing methods $m \in M$, and the one with the minimum variance score was selected as the final one, see formula (8). The frequency of the pre-processing methods *m* used for the final estimation is provided in Fig. 11. The three positions in the labels in Fig. 11 represent respectively the values $\alpha = \{2, 3, 4\}$, $diff = \{0, 1\}$ and $c = \{0, 1, 2, 3, 4\}$ (see Section 2.5 for a detailed explanation). No image pre-processing and α equal to 2 or 4 were the most common combinations considered in the final estimation. Image pre-processing was also applied a considerable number of times and therefore shows the benefits of analysing different pre-processing techniques.

3.3. Variance score calculation and optical flow velocity

The boxplots of the variance scores *r* for the points in the different data streams and the relationship between median values of the variance scores and the windiness coefficients are provided in Fig. 12. The variance scores of the cases with high windiness coefficients (Šušvė all surfaces) reached higher values compared to those with low windiness coefficients (Mūša-S1, Mūša-S2, Jūra S3). On the other hand, wind is not the only factor that affects the reliability of the results. This is clearly illustrated by the fact that cases with small windiness coefficients had a high median variance score at turbulent surfaces (Jūra-S1, Jūra-S2). The best example is the Jūra-S3 surface, which differed from the other two in its median and the amplitude of the variance score. For the mentioned surface, almost 40 % of the video area was shaded by trees and consisted of the reflection of the clouds and a lot of rippling on the water surface,

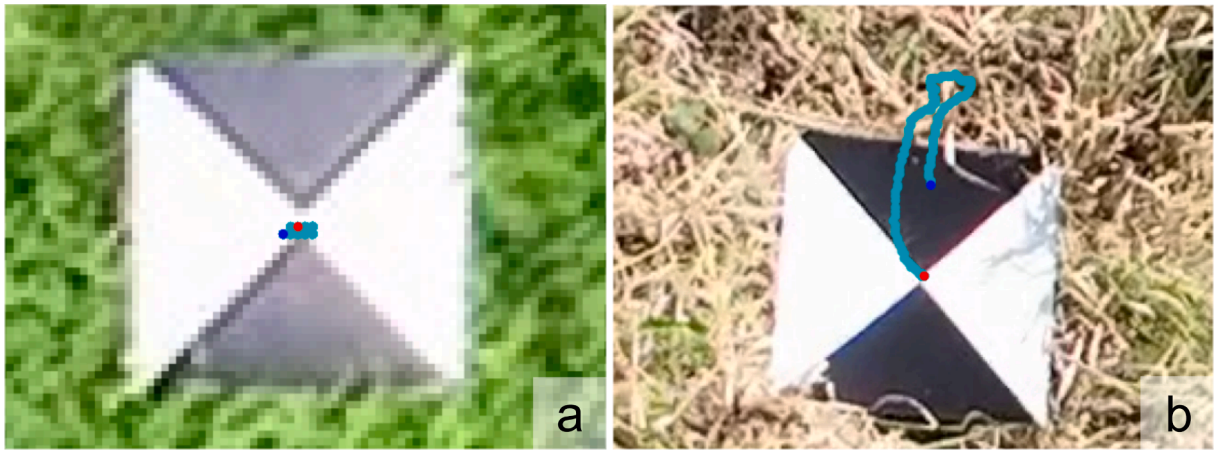

Fig. 10. Cases of movement visualisation with minimum and maximum windiness coefficient: a) Mūša-S2 (0.62); b) Šušvė-S1 (8.03).

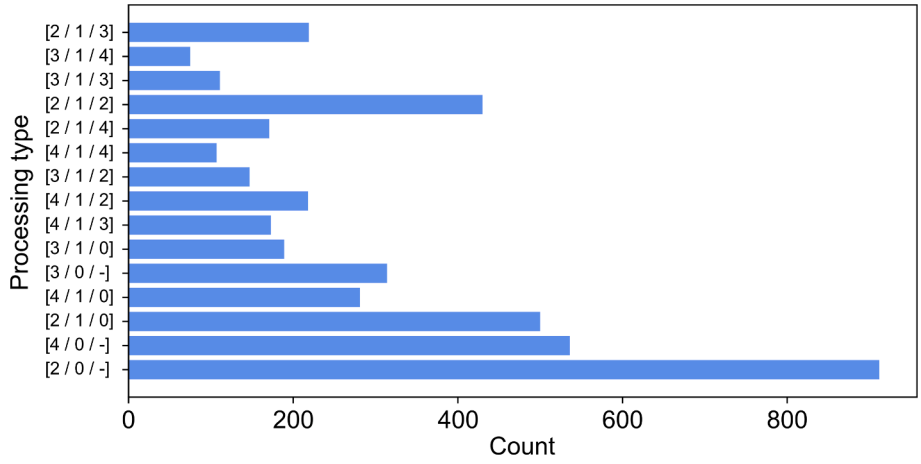

Fig. 11. Distribution of the selected pre-processing methods, the first, second, and third positions represent α, diff, and c values respectively.

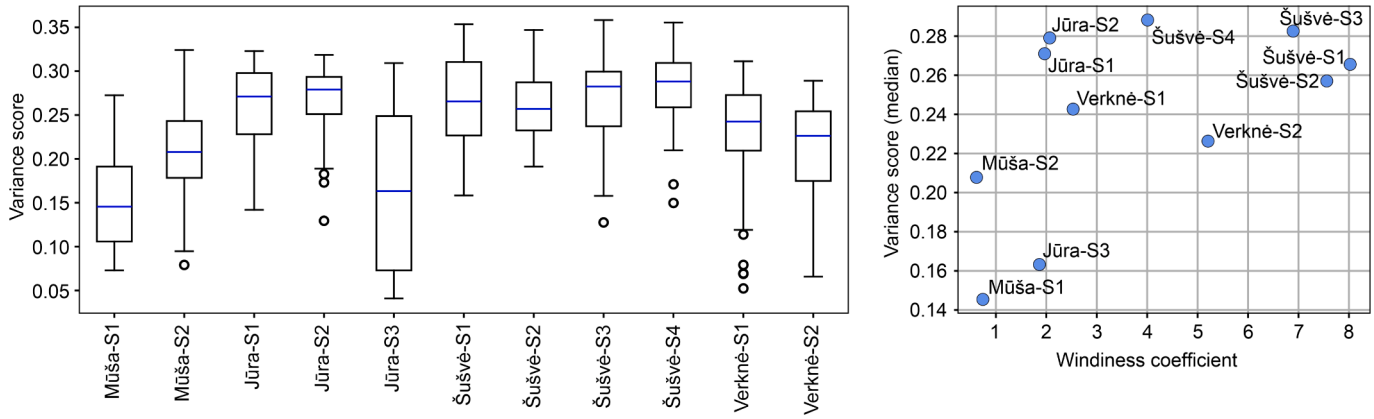

Fig. 12. Boxplots of the variance score for the points in different data streams (left), and plot of relation between median variance score and windiness coefficient for different data streams (right).

which increased the amplitude, but the remaining area had a lot of particles to track, which improved the median of the final result. The Jūra River surfaces with high median variance (S1 and S2) were characterised by turbulent water flow patterns. The relationship between the median variance score and the windiness coefficient was well expressed when considering the exceptional cases described above, such as Jūra-S1 and Jūra-S2. In addition, Mūša-S2 was characterised by its turbulence, so that the variance value increased with a similar windiness coefficient compared to Mūša-S2. For the Verknė River, the difference resulted from the reduction of the study area, with Verknė-S1 representing a larger area and Verknė-S2 being a detailed part of S1 by reducing the flight height from 21.9 to 16.2 m above the surface. These results draw attention to the selection of the target surface, which has its own optical characteristics depending on the roughness and turbulence of the water

surface, scaling, weather conditions (clouds), time of day and year, shading and other surrounding features that can cause optical differences in the detection of flow velocity.

Fig. 13 demonstrates the estimated velocity field for the cases of minimum (Fig. 13a) and maximum (Fig. 13b) variance scores, represented by the median value of the variance score of the points in the analysed surfaces. The estimated velocity vectors for Mūša-S1 showed a consistent decrease in velocity due to the increase in river depth. The estimates for a flow close to zero m/s reflected the barrier effect that occurs under the influence of boulders (Fig. 13a). In the case of Šušvė-S4 with a high variance score, the velocity was also close to zero at several points. However, their estimates were not consistent with the general flow pattern, which consisted of uniformly distributed velocities with low variability. In the applied optical velocity calculation, the velocity vectors obtained from analysing different pairs of frames were averaged. Therefore, the random vectors resulted in a velocity close to zero.

3.4. Optical flow velocity comparison with direct measurements

The comparison between the optically estimated flow velocity and the direct measurements was carried out taking into account the quartiles of the variance score. The mean absolute errors (MAE) of the measured and estimated velocities were compared for the points with the variance scores from different quartiles (Fig. 14). The results from the first quartile of variance showed the best performance, where the MAE was only 0.13. The optically detected flow was clearly related to the measured values in the entire velocity range from almost 0 m/s to 0.8 m/s. However, when comparing the other quartiles with the higher variance scores, the detection became worse, especially at low velocities up to 0.4 m/s. The same applies to the fourth quartile, which was characterised by the fact that most velocities up to 0.5 m/s were underestimated in the optical detection. These results reflect the diversity of the selected river surfaces with different environmental and hydraulic features, which should be taken into account to improve the final result. Most of the measured velocities that did not reach 0.4 m/s in the fourth quartile were associated with the surfaces that had the highest variance scores and windiness coefficients during optical detection. These conditions once again draw attention to the surfaces where the reliability of the collected data was questionable.

Fig. 14 shows that a higher variance score means lower reliability and thus higher MAE values. The tendency for the optically estimated flow values to be lower than the measured values is also particularly evident in the untrustworthy results (Fig. 14d). These values can therefore be excluded from the analysis as not reliable. Fig. 15 represents the optically estimated velocities for several river segments. Only velocity vectors whose variance score is below the median value were visualised in order to present reliable results. The example of the Šušvė-S4 surface clearly indicated the case where only some optically detected flow velocity estimates fall within the range of reliable data at the locations of the point measurement. This tendency illustrates the high variance score in practise and how this value defines unreliable data. On the other hand, other surfaces, such as Mūša-S2 and Jūra-S3, showed better performance of optically detected flow velocities, where most of the estimated values were considered as reliable. In addition, the instream roughness due to aquatic vegetation or near the river banks or the boulder effect was common in all studied river sections and was associated with unreliable data. The same was found for the Verknė-S1 surface, which was characterised by dense aquatic vegetation in the middle of the riverbed. These vegetation areas shaded the flow patterns so the velocity values reached the threshold for variance score threshold and were considered as unreliable. Of course, the variance score assessment threshold could also be set in other ways, e.g. by defining an

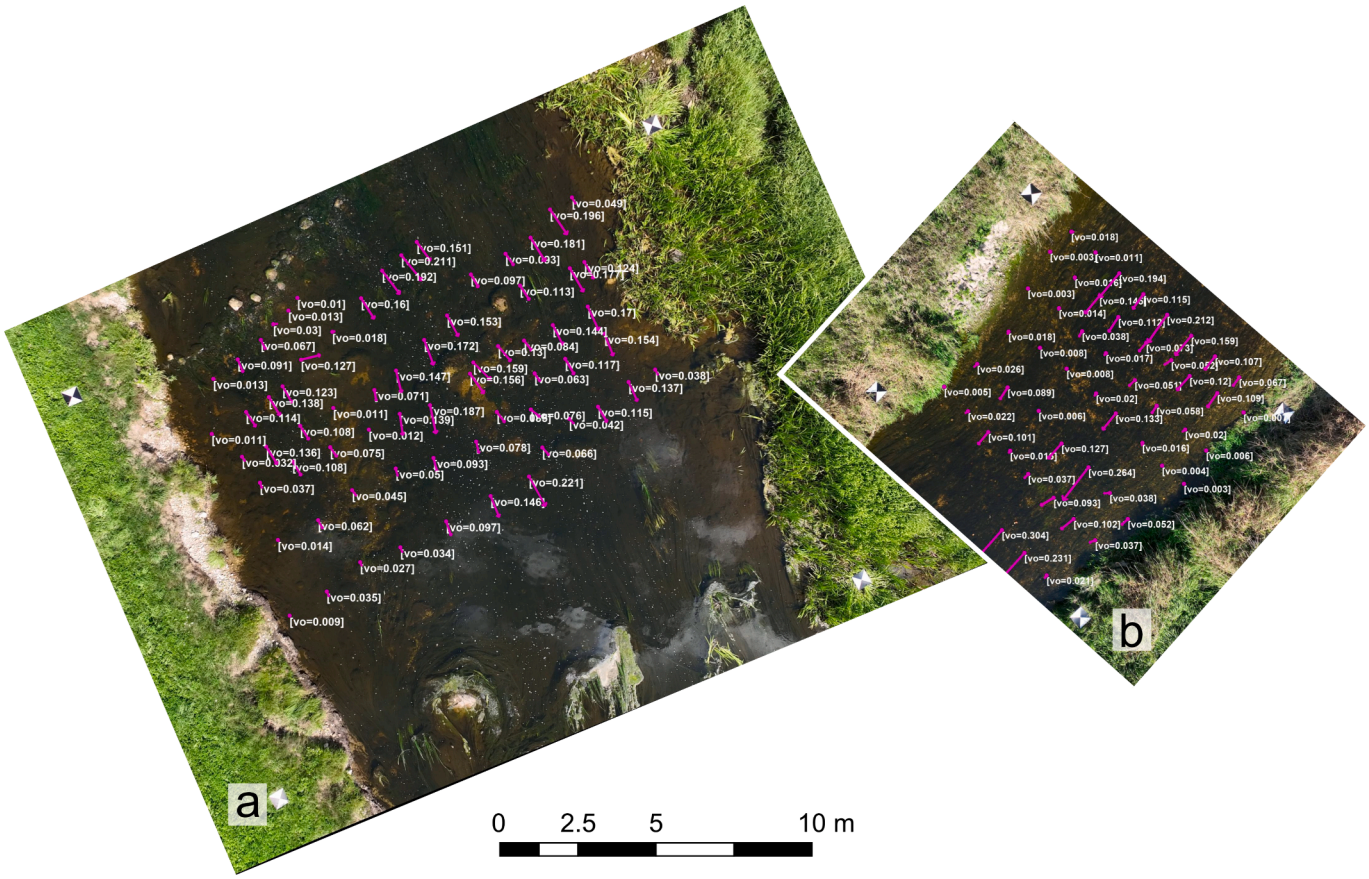

Fig. 13. Velocity field of the cases with minimum (a) Mūša-S1, 0.14) and maximum (b) Šušvė-S4, 0.29) variance scores.

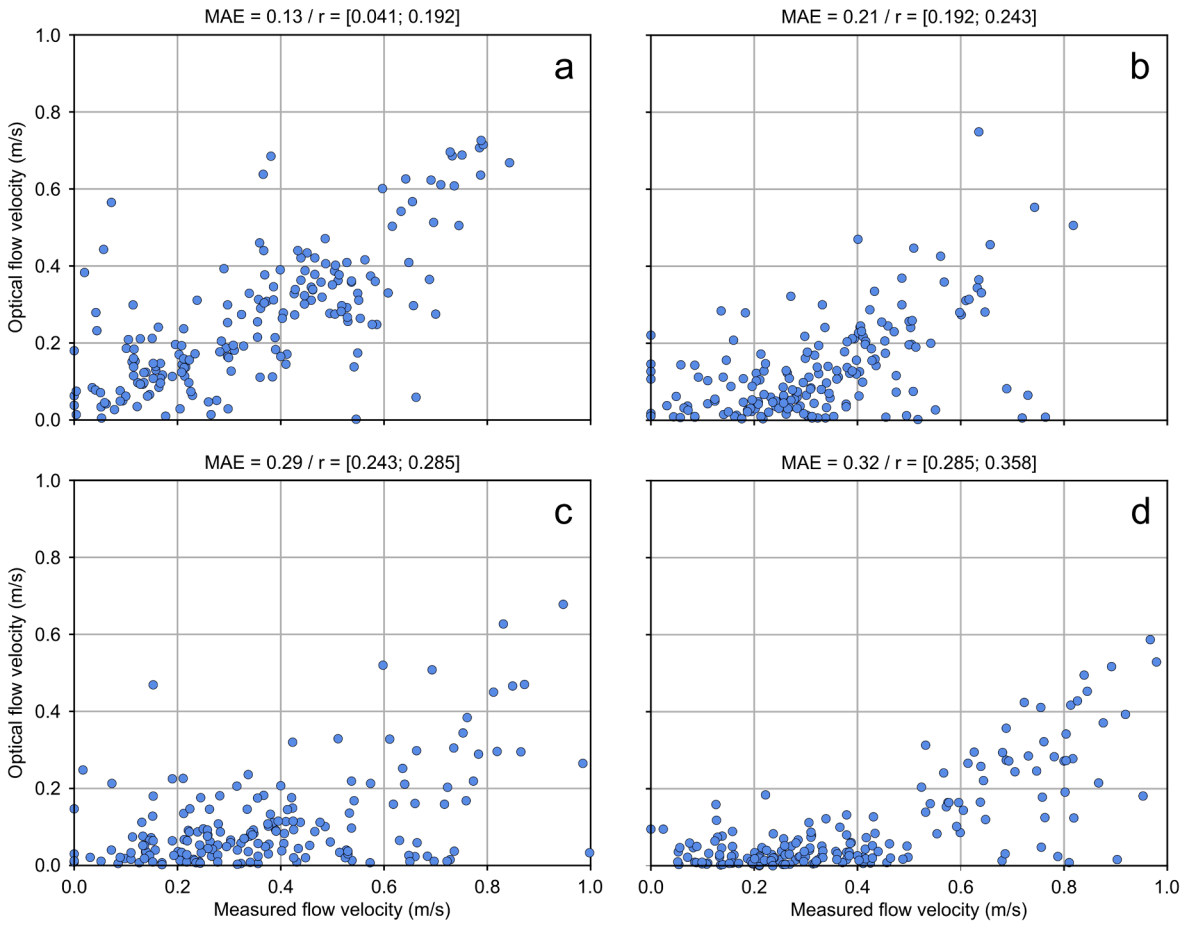

Fig. 14. MAE of optically estimated and directly measured flow grouped in quartiles regarding the variance score: a) Q1; b) Q2; c) Q3; d) Q4.

acceptable accuracy. However, the measurement and the optical flow may differ due to physical characteristics, as the measurements were taken 0.1 m below the water surface and consist of scalar data only.

4. Discussion

Research into the development of unmanned aerial vehicles (UAVs) and their measurement technologies is taking place on various fronts and at many levels (Tosi et al., 2020). Scientists are closely examining various aspects of the optical detection process, uncovering complicated relationships and proposing innovative and more effective solutions for processing of areal imagery. In particular, the optical measurement of river flow velocity is characterised by its numerous advantages over direct measurement methods (Koutalakis and Zaimes, 2022; Jyoti et al., 2023). First and foremost, the use of UAV technology enables the recording of videos in otherwise inaccessible or difficult landscapes and overcomes the limitations of direct measurement methods (Laghari et al., 2023). Furthermore, the integration of automated velocity estimation enables the rapid processing of large datasets, facilitating the analysis of extensive river sections within a reasonable timeframe (Eltner et al., 2021). This automated approach not only increases efficiency but also minimises human intervention, thus reducing 'operational' costs (Laghari et al., 2023). However, direct measurement is a conventional technique whose results can be considered ground truth with much higher accuracy (Akstinas et al., 2022). In this study, our results emphasise the sensitivity of optical detection methods implemented in modern software frameworks, especially under various hydraulic conditions of the river surfaces. The results were assessed using the median values of the variance score, with the lowest variance in this study defining to the most reliable results. The proposed variance score provides a quantitative method for evaluating the accuracy of the optically detected flow velocities. Additionally, techniques such as a constant threshold can also be applied. We not only point out these challenges, but also explore strategies to mitigate them by either addressing the underlying problems directly, developing alternative methods, or refining existing solutions. For example, Khalid et al. (2019) have shown that optical flow is suitable for tracking the movement of the river surface and emphasised the importance of accurate reconstruction of the trajectory despite sensitivity to outliers and systematic errors. Their study demonstrated the ability to reconstruct trajectories similar to reference paths and identified large-scale rotational movement patterns caused by river flow around obstacles.

Environmental factors significantly limit monitoring approaches, especially those that are sensitive and vulnerable for hydrometeorological events. High-tech tools are water resistant at various degrees, but in rainy weather their application is limited to a certain threshold of event severity. Drones, despite their technical characteristics, are primarily suitable for good weather conditions, with exceptions where there are technical limitations. Approaches based on image analysis remain susceptible to environmental variables such as wind and light conditions (Burdziakowski and Bobkowska, 2021). Jyoti et al. (2023) drawn attention on the image resolution and light conditions that the pixel displacement should be above two pixels in order to generate more accurate flow velocity estimation during good visibility. Whereas ambient light conditions cause the ability to estimate water surface state based on drone imagery (Flynn and Chapra, 2014). But these conditions require to be evaluated separately with additional light sensors considering all possible ranges of the lighting conditions at the same hydraulic state. Surface velocity is also highly influenced by external factors such as wind, which can alter the fixed ratios between surface

Fig. 15. Rivers stretches (a – Mūša-S2, b – Šušvė-S4, c – Jūra-S3, and d – Verknė-S1) with optically determined flow velocity at measured points, where the green arrows represent velocity directions with a variance score less than 0.245, red points represent cases with a higher variance score (unreliable). (For interpretation of the references to colour in this figure legend, the reader is referred to the web version of this article.)

and average flow velocity, known as velocity coefficients (Eltner et al., 2020), as it is advisable to avoid measuring surface velocity in windy conditions. An improvement in measurement accuracy and reliability can be achieved by increasing the seed density with detectable particles (Detert et al., 2017). However, only natural particles were used in this study, which did not cover the entire cross-section of the river, resulting in data gaps that made it difficult to derive all flow values from the sparsely distributed velocity vectors. Bandini et al. (2022) also concluded that the measurements have a low reliability, especially in situations where the roughness of the water surface is mainly caused by wind. Challenges include limitations due to different environments, wind-induced changes in the measurement of surface velocities and the need for improved measurement accuracy under complex natural conditions, especially in strong winds.

Wind is a common phenomenon that can occur quickly and significantly affect flight and measurement accuracy (Wang et al., 2019). The assessment of windiness was a crucial factor in this study for the determination of the optically based flow velocity, as it had a significant impact on the perception of the variance score of the estimated flow velocities assessing the reliability of the results. It was proposed to use the windiness coefficient based on the migration of the ground control points within the selected frames of the video stream. This approach revealed the environmental influences caused by the wind, which significantly affected the position of the drone during the stationary video recording. In some cases, the exact position of the drone was difficult to maintain despite the RTK flight support during the field surveys. Accordingly, the study sites with a higher windiness coefficient showed poorer flow velocity detection and a higher score of variances. Unfortunately, the wind conditions were not measured during the field surveys, and there was a lack of understanding of how important this parameter is for determining the flow velocity, even during seemingly smooth flight. Therefore, measuring the actual wind conditions (at a

specific measurement time) would be beneficial for a more accurate estimation of the flow velocity of the river under various wind conditions. For example, recent studies have proposed the use of drones equipped with different anemometer technologies to perform short-term wind speed measurements in the atmospheric boundary layer (Thielicke et al., 2021). In summary, the lack of wind measurements during the field surveys emphasises the importance of including this parameter to improve the accuracy of flow velocity estimation based on optical approaches. Future research should consider it and focus on comparing the actual wind conditions with the windiness coefficients derived from the drone footage to improve the reliability of the data and the accuracy of the flow velocity.

This study provided important insights into the selection of video streams and emphasised the importance of capturing footage at the certain time periods (e.g., 5 s videos with 5 s time gap) to mitigate systematic biases associated with continuous recording. The proposed framework opens up future research pathways in related topic by suggesting to automate the analysis of the entire video to identify the time periods with the lowest windiness coefficients and variance score, and thus apply them to increase the accuracy of flow velocity determination. Therefore, factors such as video sampling, *ortho*-rectification parameters, motion analysis settings and applied filters can significantly influence velocity measurements (Bodart et al., 2022). In addition, the current optical flow detection model can be refined with river-specific data so that indicators can be customised to specific environmental requirements. Several studies (Dal Sasso et al., 2021; Alongi et al., 2023), including the present one, have shown that focussing processing on a strategically selected, well-defined part of the recorded video significantly improves the performance of Large-Scale Particle Image Velocimetry, including seeding and recording, image pre-processing and post-processing. This targeted approach not only reduces the computational effort, but also improves the accuracy and reliability of the flow velocity measurements. In addition, the future can be extended by including measurements of flow direction as the current ground truth data does not consist of velocity vectors. Therefore, the study was limited to comparing only scalar values and evaluating the validity of velocity directions based on expert opinion only. Considering the measured velocity vector would facilitate the interpretation of the results. In response to this finding, our study proposes an innovative methodology that accounts for the unique characteristics and spatio-temporal variability of tracer particles throughout the video dataset. These results underline the importance of customised data processing strategies to improve the capabilities of optical flow analysis techniques for flow research.

5. Conclusions

This paper presents a novel view to methodology for determining the river flow velocity at the surface using the recurrent neural network architecture RAFT for optical flow and convolutional operations for image pre-processing. By analysing various combinations of image pre-processing techniques and areas of interest, the methodology identifies the optimal combination for specific environmental conditions. The approach not only determines the direction of the flow velocity, but also evaluates its reliability using a variance score that allows inconsistent velocity vectors to be filtered out during the analysis period.

The methodology was validated by numerical experiments carried out on video streams from four shallow rivers in Lithuania. The results were compared with direct measurement data collected during field surveys. The experiments showed that the optically estimated velocity closely matched the directly measured surface velocities with a low variance score, proving the suitability of the method for preliminary estimation of flow velocity in rivers.

The Mean Absolute Error (MAE) calculated for the quartile of data points with the lowest variance score was 0.13. This MAE was significantly lower – 1.6, 2.23, and 2.46 times – compared to the MAEs for data points from the second, third, and fourth quartiles, respectively. This highlights the methodology's effectiveness in providing accurate surface flow velocity with high reliability at the river surfaces with low variance score.

The proposed methodology for estimating river flow velocity utilises the strengths of recurrent neural networks and convolutional operations and provides a robust and reliable tool for environmental monitoring. The results of the study emphasise the importance of selecting appropriate image pre-processing techniques and highlight the benefits of variance evaluation to improve measurement accuracy. This study contributes to hydrological studies by providing a practical and efficient method for estimating surface flow velocity that can be used in various environmental and engineering applications.

CRediT authorship contribution statement

Andrius Kriščiūnas: Writing – review & editing, Writing – original draft, Visualization, Validation, Software, Methodology, Formal analysis, Conceptualization. **Dalia Čalnerytė:** Writing – review & editing, Writing – original draft, Visualization, Validation, Software, Methodology, Formal analysis, Conceptualization. **Vytautas Akstinas:** Writing – review & editing, Writing – original draft, Visualization, Formal analysis, Data curation, Conceptualization. **Diana Meilutytė-Lukauskienė:** Writing – review & editing, Writing – original draft, Data curation. **Karolina Gurjazkaitė:** Investigation, Data curation. **Rimantas Barauskas:** Writing – review & editing, Software, Project administration, Methodology.

Declaration of competing interest

The authors declare that they have no known competing financial interests or personal relationships that could have appeared to influence the work reported in this paper.

Data availability

Research data are available upon a reasonable request.

Acknowledgements

This research was funded by the Research Council of Lithuania (LMTLT) under the programme of Researcher Groups' projects, the scientific study 'Development of combined physical behavior and artificial intelligence models to determine hydromorphology of rivers by indirect measurements (ArtHyReS)' (Agreement Number S-MIP-23-88).

References

Akstinas, V., Kriščiūnas, A., Šidlauskas, A., Čalnerytė, D., Meilutytė-Lukauskienė, D., Jakimavičius, D., Fyleris, T., Nazarenko, S., Barauskas, R., 2022. Determination of river hydromorphological features in low-land rivers from aerial imagery and direct measurements using machine learning algorithms. Water 14, 4114. https://doi.org/10.3390/w14244114.

Alongi, F., Pumo, D., Nasello, C., Nizza, S., Ciraolo, G., Noto, L.V., 2023. An automatic ANN-based procedure for detecting optimal image sequences supporting LS-PIV applications for rivers monitoring. J. Hydrol. 626, 130233 https://doi.org/10.1016/j.jhydrol.2023.130233.

Bandini, F., Frías, M.C., Liu, J., Simkus, K., Karagkiolidou, S., Bauer-Gottwein, P., 2022. Challenges with regard to unmanned aerial systems (UASs) measurement of river surface velocity using doppler radar. Remote Sens. (Basel) 14, 1277. https://doi.org/10.3390/rs14051277.

Bjerklie, D.M., Birkett, C.M., Jones, J.W., Carabajal, C., Rover, J.A., Fulton, J.W., Garambois, P.-A., 2018. Satellite remote sensing estimation of river discharge: application to the Yukon River Alaska. J. Hydrol. 561, 1000–1018. https://doi.org/10.1016/j.jhydrol.2018.04.005.

Bodart, G., Le Coz, J., Jodeau, M., Hauet, A., 2022. Quantifying the operator effect in LSPIV image-based velocity and discharge measurements. EGU General Assembly Conference Abstracts. https://doi.org/10.5194/egusphere-egu22-4457.

Burdziakowski, P., Bobkowska, K., 2021. UAV photogrammetry under poor lighting conditions—accuracy considerations. Sensors 21, 3531. https://doi.org/10.3390/s21103531.

Cao, Y., Wu, Y., Yao, Q., Yu, J., Hou, D., Wu, Z., Wang, Z., 2022. River surface velocity estimation using optical flow velocimetry improved with attention mechanism and position encoding. IEEE Sensors J. 22, 16533–16544. https://doi.org/10.1109/JSEN.2022.3186972.

Dal Sasso, S.F., Pizarro, A., Manfreda, S., 2021. Recent advancements and perspectives in UAS-based image velocimetry. Drones 5, 81. https://doi.org/10.3390/drones5030081.

De Schoutheete, F., Carlier D'Odeigne, O., Soares-Frazão, S., 2019. DRONE-DRIVEN SURFACE VELOCITY MEASUREMENTS IN NATURAL RIVERS. Presented at the 38th IAHR World Congress, pp. 1137–1144. 10.3850/38WC092019-0782.

Detert, M., Johnson, E.D., Weitbrecht, V., 2017. Proof-of-concept for low-cost and non-contact synoptic airborne river flow measurements. Int. J. Remote Sens. 38, 2780–2807. https://doi.org/10.1080/01431161.2017.1294782.

Di Baldassarre, G., Montanari, A., 2009. Uncertainty in river discharge observations: a quantitative analysis. Hydrol. Earth Syst. Sci. 13, 913–921. https://doi.org/10.5194/hess-13-913-2009.

Eltner, A., Mader, D., Szopos, N., Nagy, B., Grundmann, J., Bertalan, L., 2021. USING THERMAL AND RGB UAV IMAGERY TO MEASURE SURFACE FLOW VELOCITIES OF RIVERS. Int. Arch. Photogramm. Remote Sens. Spatial Inf. Sci. XLIII-B2-2021, 717–722. 10.5194/isprs-archives-XLIII-B2-2021-717-2021.

Eltner, A., Sardemann, H., Grundmann, J., 2020. Technical Note: Flow velocity and discharge measurement in rivers using terrestrial and unmanned-aerial-vehicle imagery. Hydrol. Earth Syst. Sci. 24, 1429–1445. https://doi.org/10.5194/hess-24-1429-2020.

Figuérez, J.A., González, J., Galán, Á., 2021. Accurate open channel flowrate estimation using 2D RANS modelization and ADCP measurements. Water 13, 1772. https://doi.org/10.3390/w13131772.

Flynn, K.F., Chapra, S.C., 2014. Remote sensing of submerged aquatic vegetation in a shallow non-turbid river using an unmanned aerial vehicle. Remote Sens. (Basel) 6, 12815–12836. https://doi.org/10.3390/rs61212815.

Fulton, J.W., Mason, C.A., Eggleston, J.R., Nicotra, M.J., Chiu, C.-L., Henneberg, M.F., Best, H.R., Cederberg, J.R., Holnbeck, S.R., Lotspeich, R.R., Laveau, C.D., Moramarco, T., Jones, M.E., Gourley, J.J., Wasielewski, D., 2020. Near-Field Remote Sensing of Surface Velocity and River Discharge Using Radars and the Probability Concept at 10 U.S. Geological Survey Streamgages. Remote Sensing 12, 1296. 10.3390/rs12081296.

Geiger, A., Lenz, P., Stiller, C., Urtasun, R., 2013. Vision meets robotics: the KITTI dataset. The International Journal of Robotics Research 32, 1231–1237. https://doi.org/10.1177/0278364913491297.

Ho, H.-C., Chiu, Y.-W., Chen, T.-Y., Lin, Y.-C., 2023. Flow measurement in open channels using imaging techniques in conjunction with a convolutional neural network. J. Hydrol. 618, 129183 https://doi.org/10.1016/j.jhydrol.2023.129183.

Horn, B.K.P., Schunck, B.G., 1981. Determining optical flow. Artif. Intell. 17, 185–203. https://doi.org/10.1016/0004-3702(81)90024-2.

Jyoti, J.S., Medeiros, H., Sebo, S., McDonald, W., 2023. River velocity measurements using optical flow algorithm and unoccupied aerial vehicles: a case study. Flow Meas. Instrum. 91, 102341 https://doi.org/10.1016/j.flowmeasinst.2023.102341.

Khalid, M., Pénard, L., Mémin, E., 2019. Optical flow for image-based river velocity estimation. Flow Meas. Instrum. 65, 110–121. https://doi.org/10.1016/j.flowmeasinst.2018.11.009.

Kinzel, P., Legleiter, C., 2019. sUAS-based remote sensing of river discharge using thermal particle image velocimetry and bathymetric lidar. Remote Sens. (Basel) 11, 2317. https://doi.org/10.3390/rs11192317.

Koutalakis, P., Tzoraki, O., Zaimes, G., 2019. UAVs for hydrologic scopes: application of a low-cost UAV to estimate surface water velocity by using three different image-based methods. Drones 3, 14. https://doi.org/10.3390/drones3010014.

Koutalakis, P., Zaimes, G.N., 2022. River flow measurements utilizing UAV-based surface velocimetry and bathymetry coupled with sonar. Hydrology 9, 148. https://doi.org/10.3390/hydrology9080148.

Laghari, A.A., Jumani, A.K., Laghari, R.A., Nawaz, H., 2023. Unmanned aerial vehicles: a review. Cognitive Robotics 3, 8–22. https://doi.org/10.1016/j.cogr.2022.12.004.

Le Coz, J., Camenen, B., Peyrard, X., Dramais, G., 2012. Uncertainty in open-channel discharges measured with the velocity–area method. Flow Meas. Instrum. 26, 18–29. https://doi.org/10.1016/j.flowmeasinst.2012.05.001.

Legleiter, C.J., Kinzel, P.J., Nelson, J.M., 2017. Remote measurement of river discharge using thermal particle image velocimetry (PIV) and various sources of bathymetric information. J. Hydrol. 554, 490–506. https://doi.org/10.1016/j.jhydrol.2017.09.004.

Legleiter, C.J., Kinzel, P.J., 2024. A framework to facilitate development and testing of image-based river velocimetry algorithms. Earth Surf Processes Landf 49, 1361–1382. https://doi.org/10.1002/esp.5772.

Lithuanian Hydrometeorological Service under the Ministry of Environment, 2021. Assessment of climate changes in Lithuania comparing 1961–1990 and 1991–2020 Climatological Normal. LHMT Climate and Research Department, Vilnius, Lithuania. [In Lithuanian].

Mayer, N., Ilg, E., Hausser, P., Fischer, P., Cremers, D., Dosovitskiy, A., Brox, T., 2016. A Large Dataset to Train Convolutional Networks for Disparity, Optical Flow, and Scene Flow Estimation. In: In: 2016 IEEE Conference on Computer Vision and Pattern Recognition (CVPR). Presented at the 2016 IEEE Conference on Computer Vision and Pattern Recognition (CVPR). IEEE, Las Vegas, NV, USA, pp. 4040–4048. https://doi.org/10.1109/CVPR.2016.438.

Rusnák, M., Goga, T., Michaleje, L., Šulc Michalková, M., Máčka, Z., Bertalan, L., Kidová, A., 2022. Remote sensing of riparian ecosystems. Remote Sens. (Basel) 14, 2645. https://doi.org/10.3390/rs14112645.

Tauro, F., Tosi, F., Mattoccia, S., Toth, E., Piscopia, R., Grimaldi, S., 2018. Optical tracking velocimetry (OTV): leveraging optical flow and trajectory-based filtering for surface streamflow observations. Remote Sens. (Basel) 10, 2010. https://doi.org/10.3390/rs10122010.

Teed, Z., Deng, J., 2020. RAFT: Recurrent All-Pairs Field Transforms for Optical Flow. 10.48550/ARXIV.2003.12039.

Thielicke, W., Hübert, W., Müller, U., Eggert, M., Wilhelm, P., 2021. Towards accurate and practical drone-based wind measurements with an ultrasonic anemometer. Atmos. Meas. Tech. 14, 1303–1318. https://doi.org/10.5194/amt-14-1303-2021.

Tosi, F., Rocca, M., Aleotti, F., Poggi, M., Mattoccia, S., Tauro, F., Toth, E., Grimaldi, S., 2020. Enabling image-based streamflow monitoring at the edge. Remote Sens. (Basel) 12, 2047. https://doi.org/10.3390/rs12122047.

Vélez-Nicolás, M., García-López, S., Barbero, L., Ruiz-Ortiz, V., Sánchez-Bellón, Á., 2021. Applications of unmanned aerial systems (UASs) in hydrology: a review. Remote Sens. (Basel) 13, 1359. https://doi.org/10.3390/rs13071359.

Wang, Y., Chen, W., Wang, Y., 2022. Prediction and estimation of river velocity based on GAN and multifeature fusion. Comput. Intell. Neurosci. 2022, 1–10. https://doi.org/10.1155/2022/7316133.

Wang, B.H., Wang, D.B., Ali, Z.A., Ting Ting, B., Wang, H., 2019. An overview of various kinds of wind effects on unmanned aerial vehicle. Measurement and Control 52, 731–739. https://doi.org/10.1177/0020294019847688.

Wijaya, F., Liu, W.-C., Suharyanto, Huang, W.-C., 2023. Comparative assessment of different image velocimetry techniques for measuring river velocities using unmanned aerial vehicle imagery. Water 15, 3941. https://doi.org/10.3390/w15223941.

Yu, K., Lee, J., 2022. Method for measuring the surface velocity field of a river using images acquired by a moving drone. Water 15, 53. https://doi.org/10.3390/w15010053.

Zhang, Y., Yan, Z., Yang, S., Meng, W., Gu, S., Qin, J., Han, Y., Hong, Z., 2022. Research on shore-based river flow velocity inversion model using GNSS-R raw data. Remote Sens. (Basel) 14, 1170. https://doi.org/10.3390/rs14051170.